# Single Step Synthesis of Glutamic/tartaric Acid-stabilised $Fe_3O_4$ Nanoparticles for Targeted Delivery Systems

**VLADIMIR LUCIAN ENE[1-4], IONELA ANDREEA NEACSU[1-4]*, OVIDIU OPREA[1,2], VASILE ADRIAN SURDU[1-3], ROXANA DOINA TRUSCA[1-3], ANTON FICAI[1-4], ECATERINA ANDRONESCU[1- 4]**

[1]University Politehnica of Bucharest, Faculty of Applied Chemistry and Materials Science, 1 Polizu Str., 011061, Bucharest, Romania

[2]National Research Center for Food Safety, University Politehnica of Bucharest, 313 Splaiul Independentei, 060042, Bucharest, Romania

[3]National Centre for Micro and Nanomaterials, University Politehnica of Bucharest, 313 Splaiul Independentei, 060042, Bucharest, Romania

[4]Academy of Romanian Scientists, 54 Splaiul Independentei Str., 050085, Bucharest, Romania

*This paper aims to improve medical strategies regarding cancer treatment, by developing new targeted cancer therapy nanostructured systems, based on magnetite and natural catabolism products as coating agents (glutamic acid, tartaric acid), with induced cellular internalization. In order to create hydrophilic, biocompatible systems, suitable for targeted cancer therapy, and minimize the negative side effects of current approaches, a one-pot synthesis by co-precipitation technique, starting from $Fe^{2+}$ and $Fe^{3+}$ inorganic precursors and multifunctional organic compounds, carefully controlling the reaction parameters (concentration of precursors, pH, temperature etc.) was performed. The obtained $Fe_3O_4$ stabilised nanoparticles were subjected to morphological and structural characterization. The formation of inorganic-organic hybrid systems was evaluated using FTIR spectroscopy and complex thermal analysis (TG / DSC) for determining the content of the organic component, while X-ray Diffractometry and Scanning and Transmission Electron Microscopy were used to characterize the crystallinity and particle dimensions and distribution. The magnetic properties at room temperature were also evaluated, recording the magnetic susceptibility relative to the applied magnetic field.*

*Keywords: magnetite, glutamic acid, tartaric acid; stabilised magnetic nanoparticles*

Among the various magnetic nanoparticles (MNPs) used as nanocarriers for delivery of chemotherapeutic agents, $Fe_3O_4$ nanoparticles have attracted special attention because they provide opportunities for bioapplications due to their superparamagnetism [1-3]. Nevertheless, there are some *major drawbacks that limits their practical applications*: (i) bare $Fe_3O_4$ nanoparticles are highly susceptible to acidic and oxidative conditions and (ii) the existence of strong van der Waals and magnetic attractions between particles, which might cause the MNPs dispersion to be very unstable and all particles to be prone to aggregation, therefore coating an outer protective layer is very important to maintain the stability of the magnetic component [4-5]. An effective strategy to achieve this is by encapsulating $Fe_3O_4$ nanoparticles in an inorganic shell (C [6], $SiO_2$ [1,5,7], ZnO [8] etc.) to form magnetic nanocomposites, which can extend their technical application as a result of unique characteristics of the shell (high stability under extreme conditions and naturally porous structure) and their ability to provide a platform for chelating groups [9]. However, the usage of these systems for cancer treatment is limited due to the hydrophobic character that the $Fe_3O_4$@organic nanostructures usually present, proving to be extremely disadvantageous relative to their bioapplications in an aqueous environment [10].

The functionalization is extremely important for assuring chemical stability in certain body fluids, as well for obtaining the desired hydrophilic/hydrophobic balance, adsorption of certain biological active agents or in order to increase the penetrability/internalization in certain cells/tissue etc. The use of PEG as hydrophilic, highly water soluble, biocompatible, nonantigenic, and protein-resistant polymer, the so called PEGylating, is extremely attractive for obtaining magnetic systems with appropriate chemical stability in body fluids [11]. According to Tai et al. [12] PEG stabilised MNPs exhibited high colloidal stability up to 21 days as compared to the unmodified MNPs. Depending on the application, this long term stability is not necessarily needed, the cytostatic release occurring in only few days, therefore finding suitable novel coating agents is still a *limitation of current approaches*.

Based on the literature data, we propose the use of aminoacids [13-14] (e.g. glutamic acid) or hydroxiacids [15-16] (e.g. tartaric acid) as functionalization agents, leading to an increased stability and good penetrability/internalization inside the tumor. These $Fe_3O_4$@organic acid nanostructures will be further exploited as targeted delivery systems in cancer treatment, the active components being attached via different interactions between them and the stabilization agents.

*email: neacsu.a.ionela@gmail.com*

## Experimental part

*$Fe_3O_4$ synthesis*

Using the co-precipitation method described below (Figure 1), the synthesis of magnetite nanoparticles was performed as follows:

For obtaining 3g of magnetite, 3.6g of $FeSO_4 \cdot 7H_2O$ and 4.2g of $FeCl_3$ are solubilized in 600mL of deionized water under continuous magnetic stirring. Another solution is obtained by solubilizing 4.5g of NaOH in 300mL deionized water, thus providing an alkaline *p*H, required for the co-precipitation process. The first solution containing iron ions is added over the NaOH solution, dropwise, by keeping a constant flow with a peristaltic pump. At the end of the process, the accelerated decantation of the magnetite nanoparticles is carried out by placing the beaker above a magnet. After settling, keeping the magnet under the beaker in the same position relative to it, the liquid phase is removed. The precipitate is washed with ultrapure water to remove the by-products and unreacted starting materials until a neutral pH is obtained and no chloride can be identified by $AgNO_3$ in the effluents. After washing, the nanoparticles are dried in an oven at 60°C for 24 h. The obtained powder is forward referenced as *pure magnetite*.

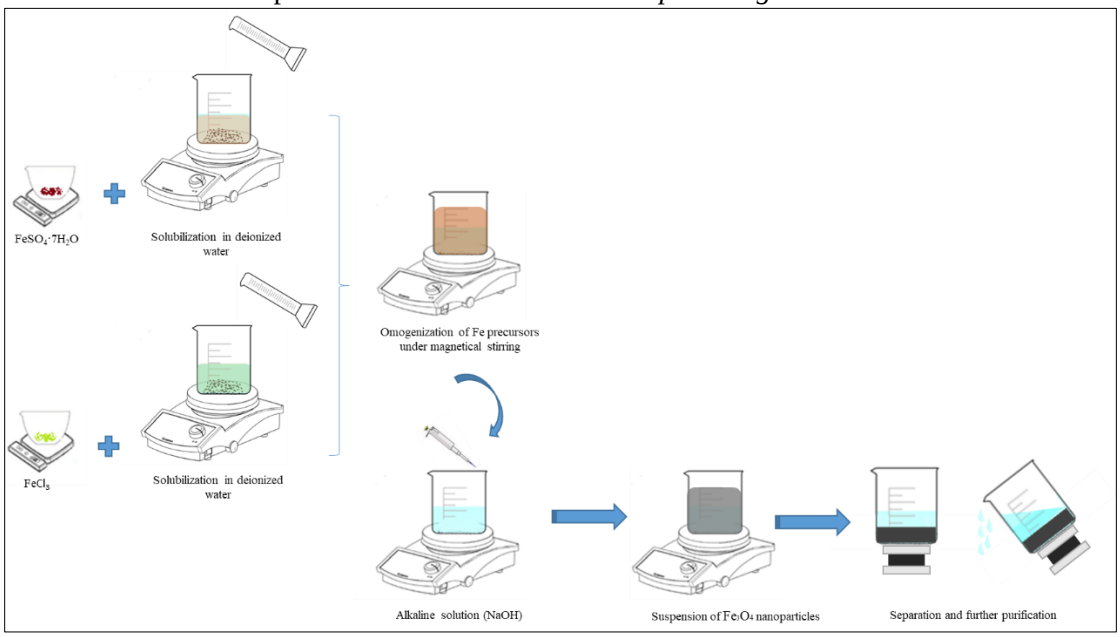


Fig. 1. Synthesis scheme of pure magnetite

*$Fe_3O_4$-glutamic acid and $Fe_3O_4$-tartaric acid*

The synthesis of glutamic acid / tartaric acid stabilised magnetite nanoparticles was performed by the modified co-precipitation route (Figure 2). The method is similar with the synthesis of magnetite, with one exception: the glutamic acid / tartaric acid is dissolved in the iron precursors solutions before adding them to the alkaline solution. The obtained powders are forward referenced as glutamic / tartaric acid stabilised magnetite and ($Fe_3O_4$@Glutamic acid, $Fe_3O_4$@Tartaric acid).

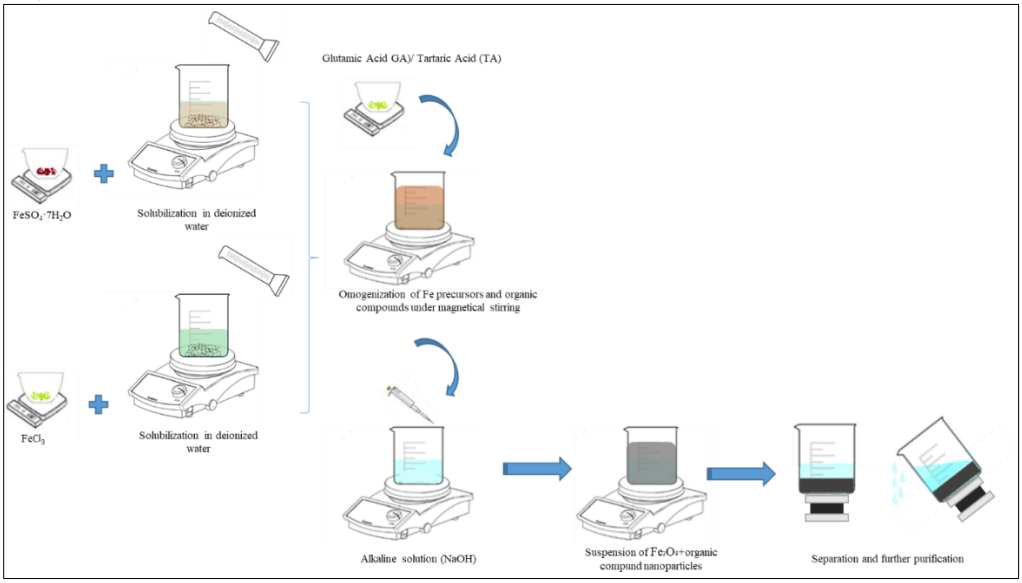


Fig. 2. Synthesis scheme of glutamic / tartaric acid stabilised magnetite

***Characterization methods***

X-ray diffraction analysis (XRD) was performed in order to characterize the materials synthesized from the point of view of their crystallinity as well as of the component phases.

XRD analysis was performed using a PANalytrical Empyrean equipment in Bragg-Brentano geometry equipped with a Cu-anode ($\lambda_{CuK\alpha}$ = 1.541874 Å) X-ray tube with in-line focusing, programmable divergent slit on the incident side and a programmable anti-scatter slit mounted on the PIXcel3D detector on the diffracted side. The analysis was acquired on the 20-80° angle range, with acquisition step of 0.02° and 100s acquisition time per step.

Scanning electron microscopy (SEM) was carried out to highlight morphology aspects of the synthesized samples and particle size. Image acquisition was performed using the High Resolution Scanning Electron Microscope, Inspect F50 at 30KeV with various magnification rates.

The Fourier-transform infrared spectroscopy (FT-IR) investigation of the synthesized powders implied the analysis of reduced sample quantities using the Nicolet iS50R spectrometer. Measurements were performed at room temperature using the Total Reflection Attenuation Module (ATR), with 32 sample scans between 4000 and 440 $cm^{-1}$ at a resolution of 4 $cm^{-1}$. The recording of spectral data was possible by connecting the spectrometer to a data acquisition and processing unit through the Omnic program.

The magnetic properties of complex nanosystems were investigated at room temperature, recording the magnetic susceptibility relative to the applied magnetic field using the vibrating sample magnetometer (VSM), LakeShore 7404.

Transmission electron microscopy (TEM) images corresponding to acid-stabilised magnetite and pure magnetite samples were obtained using a high-resolution Tecnai G2 F30 S-TWIN transmission electron microscope equipped with a Selected Area Electron Diffraction (SAED) module. The microscope operated in bright-field transmission mode at a voltage of 300 kV, with a punctual and line resolution of 2 Å and 1 Å respectively.

The thermal analysis (TG/DSC) was performed using a NETZSCH STA 449 F3 Jupiter device, heating the sample at a constant rate of 10K/min from room temperature up to 900°C in dynamic atmosphere of air with a flow of 50 mL/min.

**Results and discussions**

Following XRD analysis and data processing using the HighScore program, a single crystalline $Fe_3O_4$ (magnetite) phase was identified, according to PDF4 + [00-065-0731], with cubic structure and the crystallization planes outlined in Figure 3. The general appearance of the diffraction interferences reveals a crystalline character of the sample and small crystallite dimensions with possible particle agglomerations. In the 2θ (10-80°) range investigated, the presence of 6 specific diffraction interferences was noted, at estimated 2θ values at approximately 30, 35, 43, 54, 57 and 62°. According to the table data available in the ASTM sheets, the diffraction peaks identified for experimentally synthesized nanoparticles correspond to the diffraction planes (2 2 0), (3 1 1), (4 0 0), (4 2 2), (5 1 1), respectively (4 4 0) of the magnetite, crystallized in a cubic system.

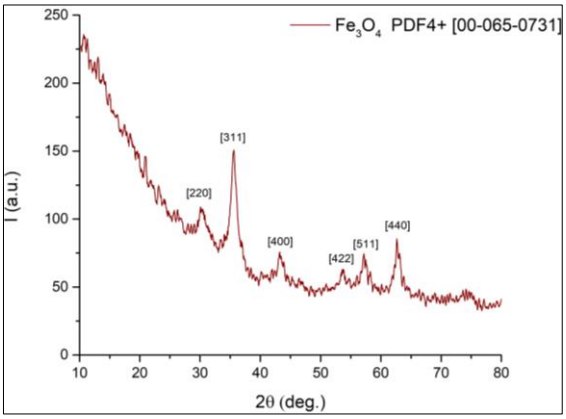


Fig.3. θ-2θ analysis performed on pure magnetite

Figure 4 shows the X-ray diffraction spectra of $Fe_3O_4$ and glutamic/tartaric acid stabilised $Fe_3O_4$ samples. Both spectra highlight the presence of the characteristic peaks of magnetite, previously detailed. The presence of tartaric acid is identified by the two characteristic diffraction interferences at 2θ of 31 and 46 (according to PDF4+ [00-031-1911]).

It is worth noting that the intensity of the diffraction interferences, in the sample containing glutamic acid, has higher values at low angles compared to the pure magnetite sample. This can be attributed to the presence of the crystalline organic phase on the surface of the magnetic nanoparticles, with diffraction peaks of 2Theta = 30 and 35° (attributed to the glutamic acid according to PDF4 + [00-019-1757]), the result being a synergistic effect of the highlighted phases.

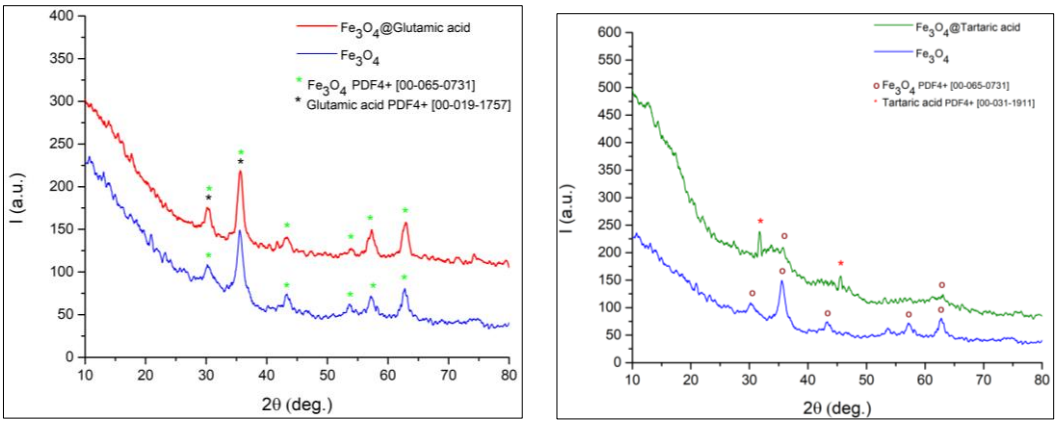


Fig. 4. θ-2θ analysis performed on pure magnetite and glutamic/tartaric acid stabilised magnetite

The scanning electron microscopy (SEM) images presented in Figure 5 are consistent with the information from the X-ray spectrum, highlighting the nanometric size of the magnetite particles obtained, with dimensions between 3 and 5 nm. It can be seen how, due to the large surface area associated with reduced size, the particles have a high tendency of agglomeration.

The reduced size of the nanoparticles and the maximum resolution of the equipment make it difficult to pinpoint the shape of the particles, which seems quasi-spherical. The organic compounds used in the synthesis process seem to have stabilised the oxide particles. However, determinations are difficult to achieve because of the presence of glutamic / tartaric acid that alters image quality. For a detailed morphological characterization that determines the mean particle size and shape, Transmission Electron Microscopy (TEM) was used.

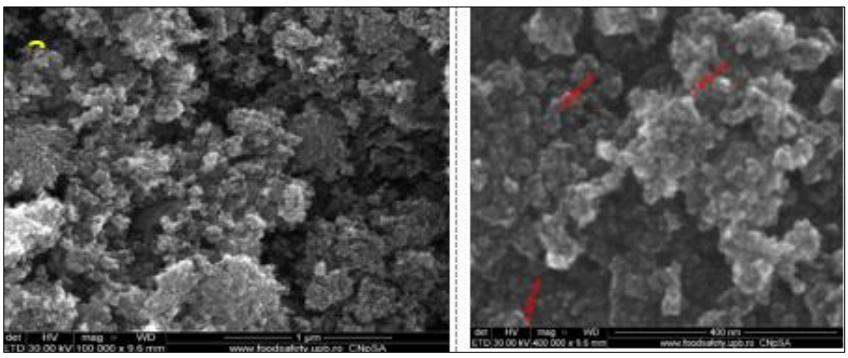

Fig. 5. SEM images of a) pure magnetite, b) glutamic acid stabilised magnetite, c) tartaric

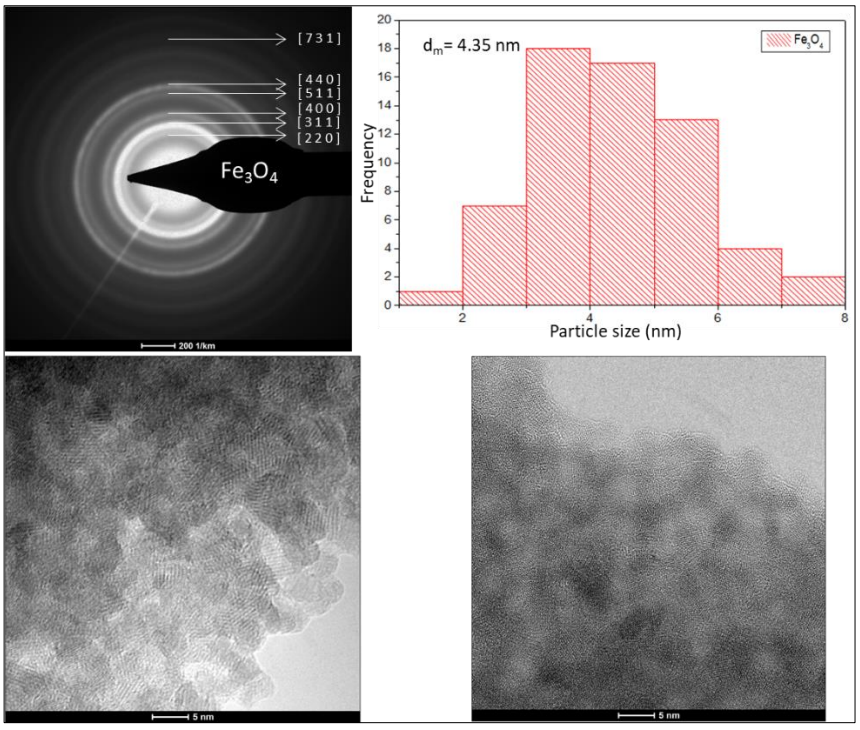


Fig. 6. HR-TEM, SAED and particle size distribution for pure magnetite

Figure 6 lists information provided by transmission electron microscopy. Thus, the bright field transmission electron microscopy (BF-TEM) image obtained for the magnetite sample shows that the sample consists of nanoparticle agglomerates with a predominantly spherical and polyhedral morphology. The mean particle size estimated by measuring 62 particles is 4.35 +/- 0.02 nm, with an unimodal distribution. Selected area electron diffraction shows well defined diffraction rings corresponding to (2 2 0), (3 1 1), (4 0 0), (4 2 2), (5 1 1) and (4 4 0) crystallographic planes. The rings are diffuse which means that the powder has a low degree of crystallinity.

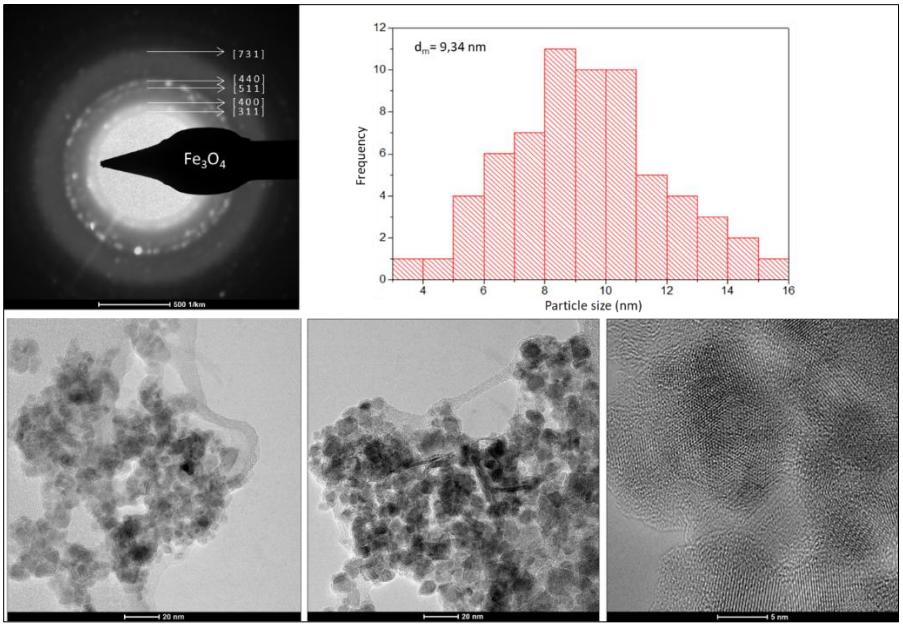


Fig. 7. TEM, HR-TEM, SAED and particle distribution of glutamic acid stabilised *magnetite*

BF-TEM measurements on $Fe_3O_4$ – glutamic acid particles mark the obtaining of hybrid core-shell nanoparticles consisting of $Fe_3O_4$ crystalline core and glutamic acid non-crystalline shell of about 1-2 nm. The overall mean particle size is 9.34 ± 0.71, higher as compared to pure $Fe_3O_4$ nanoparticles, which proves that glutamic acid is arranged uniformly around the oxide core (Figure 7). SAED pattern show diffraction rings consisting of bright diffraction spots, which show a higher degree of crystallinity than of pure $Fe_3O_4$ nanoparticles.

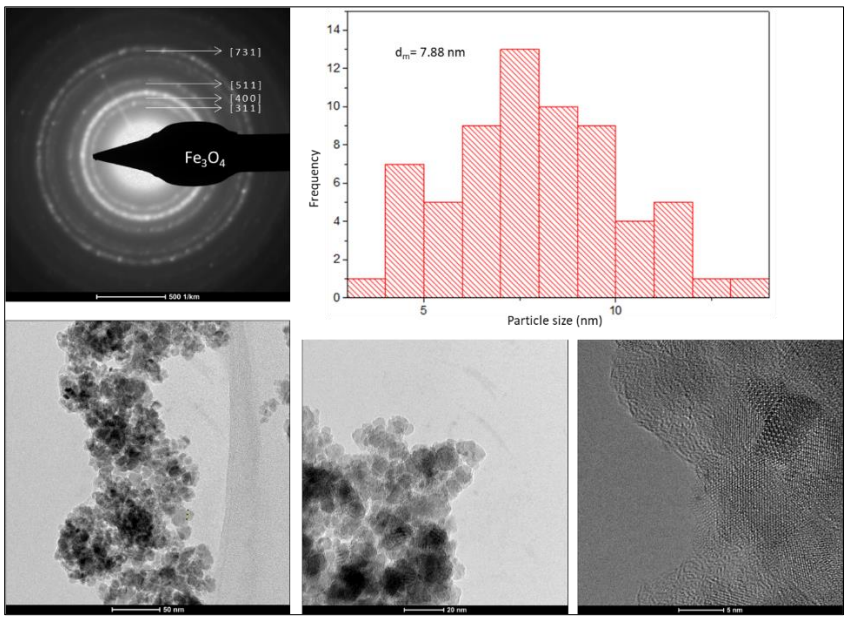


Fig. 8. TEM, HR-TEM, SAED and particle size distribution of tartaric stabilised magnetite

The transmission electron microscopy analysis shown in Figure 8 on the tartaric acid stabilised magnetite reveals the reduction of magnetite agglomerates along with the increase in the average size of the magnetite particles. These effects are due to the tartaric acid coating of magnetite particles which compensates for the free energy of the surface of the latter. The electron diffraction on the selected area highlight the magnetite specific diffraction rings. An enlargement of

the dimensional domain of the magnetite particles is observed, the particle sizes varying between 3-15 nm (mean particle size is 7.88 ± 0.57), compared to the uncovered magnetite which revealed by observation an upper dimensional limit of 7 nm. This can be explained by the presence in the medium of synthesis of tartaric acid which, on the one hand, subtly modifies the pH of the $Fe_3O_4$ formation, and on the other, alters the surface tension of the solution leading to a varied particular morphology and dimensionality.

In Figure 9, the FT-IR spectra of $Fe_3O_4$, glutamic/tartaric acid and glutamic/tartaric acid stabilised $Fe_3O_4$ are presented with the intent of comparison. In the glutamic acid spectrum, the characteristic bands are observed, in correlation with the structural formula of glutamic acid, as follows: at 3005 $cm^{-1}$ - the OH stretch vibration specific band; at 2855 $cm^{-1}$ - tensile vibration band of the CH bond; at 1690 $cm^{-1}$ - the C = O- bonding band and at 1523 $cm^{-1}$ - specific stretching band of the NH- linkage from the amino group. Spectrum of $Fe_3O_4$@Glutamic acid exhibits common elements for the two component phases, thus recalling around 550 $cm^{-1}$ of the band corresponding to the Fe-O bond of magnetite, and in the range of 1500-1600 $cm^{-1}$ - the glutamic acid-specific bands. Absorbance of the latter does not, however, record high values, possibly due to a small amount of organic phase on the surface of the oxide particles. The FT-IR spectra of the tartaric acid and tartaric acid stabilised magnetite reveal the characteristic bands of magnetite, described above in addition to absorption bands in the 1000-1750 $cm^{-1}$ range, correlated with interatomic bonds in the OH, COOH, C=O and C-O, specific to the tartaric acid. According to the FTIR spectra, stabilization with tartaric acid leads to the most important change of the FT-IR, most probably a higher content of the stabilizing agents is adsorbed onto the surface of the magnetite.

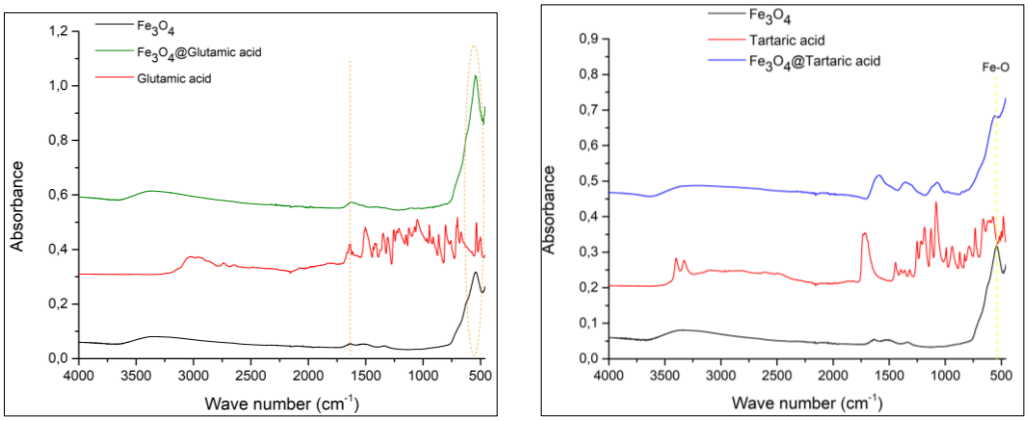


Fig. 9. FT-IR spectra of magnetite, glutamic/tartaric acid and glutamic/tartaric acid stabilised magnetite

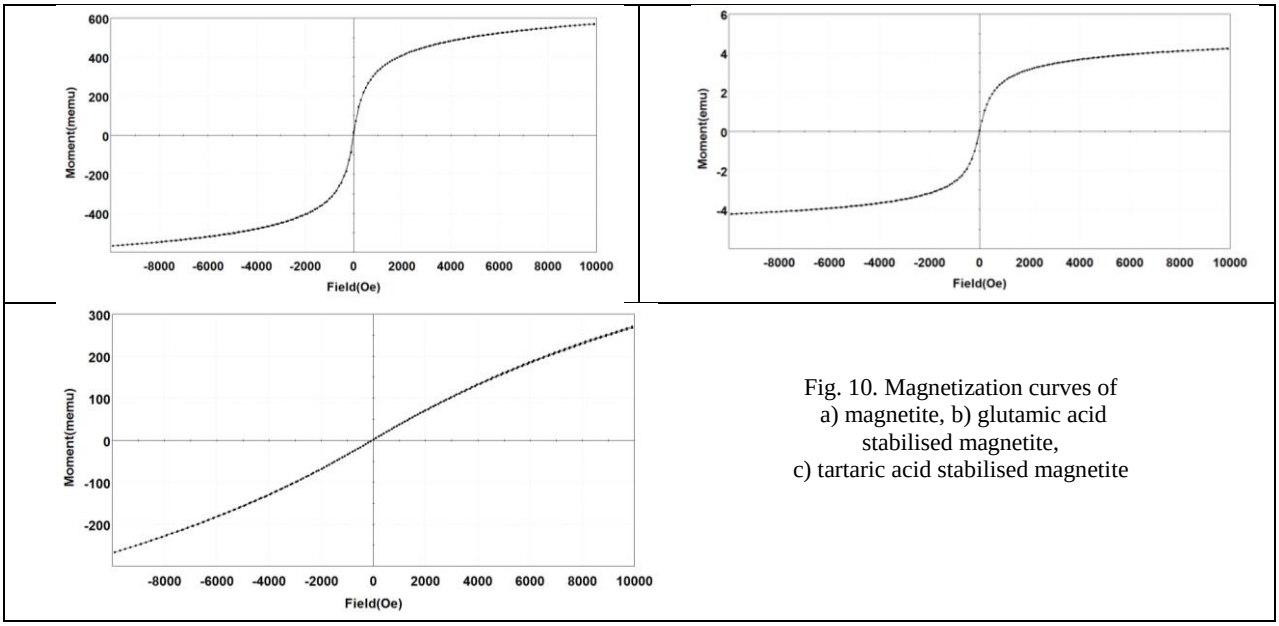


Fig. 10. Magnetization curves of a) magnetite, b) glutamic acid stabilised magnetite, c) tartaric acid stabilised magnetite

Figure 10 shows the magnetization variation according to the magnetic field applied for the pure and stabilised $Fe_3O_4$ nanoparticles at 25° C. In the range of -10 to 10 kOe of applied magnetic field, the magnetization has a significant increase, reaching the saturation value at about 9000 Oe, this behavior being characteristic to paramagnetic particles. In the case of bulk magnetite, the saturation magnetization is about 95 emu/g. High saturation magnetization can also provide electromagnetic shielding properties for hybrid coatings used in certain applications. In the biomedical domain, a saturation magnetization of 10 emu/g is sufficient for the use of magnetic nanoparticles as targeted delivery systems.

The sample possess low coercivity (12.088 Oe), indicating the superparamagnetic nature of the particles. Saturation magnetization is a linear function of the nanoparticle diameter value. The saturation magnetization value was 14.56 emu/g for the magnetite nanoparticles, therefore the synthesized magnetic nanoparticles possess the magnetic properties required in their use as complex targeted delivery systems.

A similar behavior of magnetization to applied magnetic field with the one of pure magnetite can be observed in the case of glutamic acid stabilised magnetite. The nanoparticles of $Fe_3O_4$ @ glutamic acid synthesized in this study, exhibit a saturation magnetization of 42 emu/g and possess the magnetic properties required for use as targeted delivery systems.

The tartaric acid stabilised magnetite has a superparamagnetic character that recommends it for biomedical applications. The analyzed sample has a saturation magnetization of 6.71 emu/g, 46.1 % lower than that of pristine magnetite. This decrease is due to the presence of the coating material, implicitly of the mass increase with the addition of a second component lacking magnetic properties.

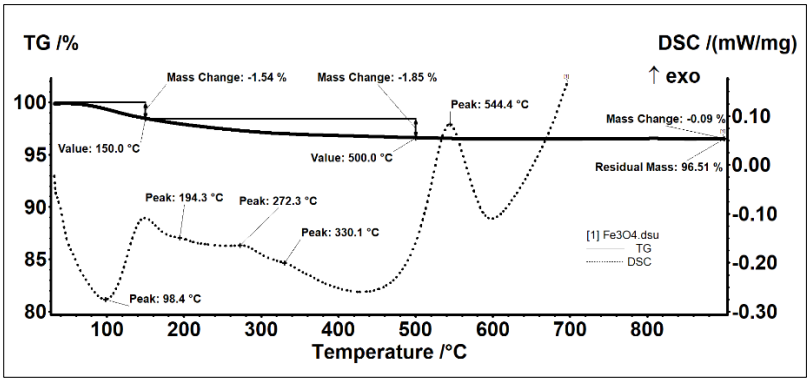


Fig. 11. Complex thermal analysis on pure magnetite

The complex thermal analysis of pristine magnetite presented in Figure 11 shows that the first mass loss (1.55%), accompanied by an endothermic effect with a minimum at 98.4°C, occurs in the range of 30-150°C. Mass loss is caused by the removal of water from the sample and possibly the loss of weakly bonded -OH groups on the surface of the nanoparticles. In the range of 150-500°C, the recorded mass loss is 1.85%, and it is accompanied by several, weak, overlapping effects. In principle, remnants traces of precursors from the synthesis of magnetite are degraded. The peak at 330°C can be attributed to magnetite transformation into maghemite (oxidation process). On the DSC curve, a slight exothermic effect at 544.4°C is observed. This is a phase transformation of maghemite into hematite. It is a specific phase transformation encountered in thermal analysis of almost magnetite samples, but the position of this peak is dependent on many factors, like: nanoparticle size, shape, synthesis method, etc. After 500°C the mass loss of 0.09% is recorded on the range 500-900°C and basically the mass remains virtually constant, the residual mass reaching representing 96.51% (and finally the sample is black- dark gray color). Over the temperature range of thermal under analysis, the two phase-specific $Fe_3O_4$ transformations, magnetite in maghemite (330°C) and maghemite in hematite (544°C), respectively, can be observed.

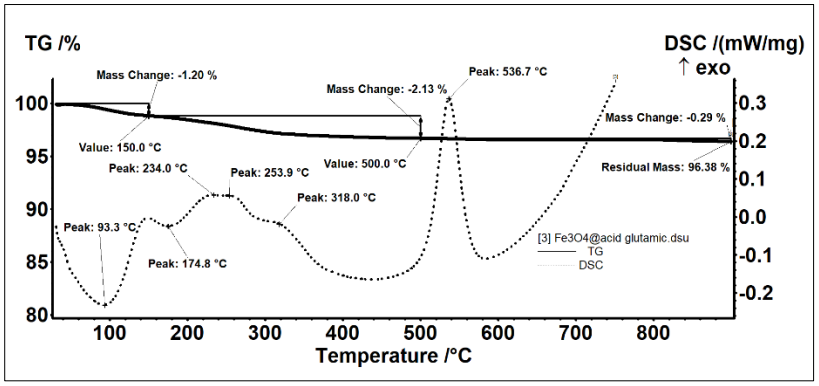


Fig. 12. Complex thermal analysis on glutamic acid stabilised magnetite

From the point of view of thermal behavior, as shown in Figure 12, the glutamic acid stabilised $Fe_3O_4$ is similar to simple magnetite, but there are a few differences though: mass loss appears to be slower in the 200°C area and the residue is reddish. The first mass loss takes place in the range of 30-150°C, 1.20% and is accompanied by an endothermic effect with a minimum at 93.3°C. Mass loss is caused by the removal of some water molecules from the sample and possibly of -OH groups on the surface of nanoparticles. The mass loss is smaller than that of pristine magnetite indicating

a smaller quantity of volatile molecules. This might be the case if the nanoparticles are stabilised with glutamic acid which replaces some of the water on surface sites.

In the range of 150-500ºC, the recorded mass loss is 2.13%, and it is accompanied by several weak, overlapped effects. This mass loss step is larger than that of pristine magnetite indicating a possible oxidative degradation of glutamic acid. The peak at 318ºC represents the transformation of magnetite into maghemite (oxidation process). On the DSC curve, a strong exothermic effect at 536.7°C is observed, corresponding to the phase transformation of maghemite into hematite. A mass loss of 0.29% is recorded over the range 500-900ºC, which again is higher than in the case of simple magnetite. The mass loss in this interval is usually due to the slow oxidation of carbonaceous mass remained after the degradation of organic coat. The residual mass is 96.38%, with a color of brownish-red.

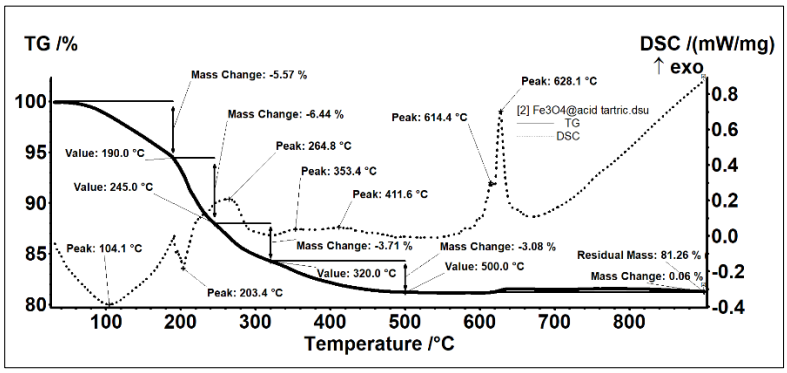


Fig. 13. Complex thermal analysis of tartaric acid stabilised magnetite

Figure 13 illustrates the thermal behavior of tartaric acid stabilised magnetite. In the 30-190°C interval, the first mass loss (5.57%) occurs, accompanied by an endothermic effect with a minimum at 104.1°C. Mass loss is caused by the removal of water from the sample and possibly of -OH groups on the surface of nanoparticles, together with other volatile molecules. Since magnetite has larger quantity of tartaric acid on its surface it is possible to retain more water compared to the simple magnetite sample. Loss of more water leads to a change in the temperature at which the endothermic peak occurs. A loss of mass of 6.44% is recorded in the range 190-245°C, accompanied by an endothermic effect with a minimum at 203.4°C. Thus, the recorded mass loss can represent a decomposition, most likely of tartaric acid or an evaporation of a volatile compound obtained thru decomposition or both. The mass loss is continuous in the range of 245-320°C (3.71%) and the process is accompanied by a slight exothermic effect with the maximum at 264.8°C. Oxidative degradation of organic residue continues in the range 320-500°C, with a mass loss of 3.08% and exothermic weak peaks at 353 and 411°C. There is then a slight increase in mass between 620-640°C. Degradation of the organic substance results in a carbonaceous residue, which partially reduces the iron from the surface of the nanoparticles. Then, after the removal of carbon, the iron is oxidized to $Fe_2O_3$ and this leads to the observed mass increase. In addition to this exothermic process, there is also the phase transformation of maghemite into hematite. The two effects are partly superimposed with maximum at 614 and 628°C. The residual mass is 81.26%, with a black-brown color.

## Conclusions

This study is focused on obtaining acid stabilised magnetite with potential uses in targeted delivery of therapeutic agents. In order to stabilize the magnetite on one hand, and on the other hand to confer mixed functional groups on its surface, one aminoacid (glutamic acid) and one hydroxiacid (tartaric acid) were used as coating agents. In order to discuss their differences, a batch of pure, unstabilised magnetite was obtained using the co-precipitation route, to use as standard, and also, two batches of glutamic acid and tartaric acid (respectively) stabilised magnetite were obtained by the same co-precipitation technique, with minor modifications.

Structural investigations emphasize the obtainment of cubic $Fe_3O_4$ and glutamic/tartaric acid stabilised $Fe_3O_4$ with a high degree of crystallinity. Morphology studies have shown, as it was expected, that in the case of pure magnetite, the tendency of particle agglomeration is larger than that of functionalized magnetite, which pointed out that individual, larger $Fe_3O_4$ nanoparticles were stabilised with the organic compound. Magnetometry measurements indicated lower values of magnetization for the stabilised particles compared to the unstabilised ones, but these values have still proven adequate for using the functionalized nanoparticles as complex targeted delivery systems. Complex thermal analysis was carried out to reveal the thermal domain in which the functionalized superparamagnetic nanoparticles are stable, and also, to offer a semi-quantitative measure of the organic compound retention on the surface of magnetite.

All the above-mentioned properties are strong premises for glutamic/tartaric acid stabilised $Fe_3O_4$ nanoparticles to act as valuable candidates in any domain that requires targeted delivery but only after complex biological assessments related to biocompatibility, bioaccumulation, internalization in cells, tissue and organs, etc.

*Acknowledgement: V. L. Ene and I. A. Neacsu highly acknowledge the grant received from* Academy of Romanian Scientists.

## References

1. MOHAMMED, L., GOMAA, H.G., RAGAB, D., ZHU, J., Particuology, **30**, 2017, p. 1.
2. UNSOY, G., GUNDUZ, U., OPREA, O., FICAI, D., SONMEZ, M., RADULESCU, M., ALEXIE, M., FICAI, A., Curr. Top. Med. Chem., **15**, 2015, p. 1622.
3. KIM, D.K., ZHANG, Y., VOIT, W., RAO, K.V., KEHR, J., BJELKE, B., MUHAMMED, M., Scr. Mater., **44**, 2001, p. 1713.
4. XU, J.K., ZHANG, F.F., SUN, J.J., SHENG, J., WANG, F., SUN, M., Molecules, **19**, 2014, p. 21506.
5. SONMEZ, M., GEORGESCU, M., ALEXANDRESCU, L., GURAU, D., FICAI, A., FICAI, D., ANDRONESCU, E., Curr. Pharm. Des., **21**, 2015, p. 5324.
6. HUANG, J., LI, Y., JIA, X., SONG, H., Tribol. Int., **129**, 2019, p.427.
7. ULU, A., OZCAN, I., KOYTEPE, S., ATES, B., In.t J. Biol. Macromol., **115**, 2018, p. 1122.
8. ATLA, S.B., LIN, W.R., CHIEN, T.C., TSENG, M.T., SHU, J.C., CHEN, C.C., Mater. Chem. Phys., **216**, 2018, p. 380.
9. GRUMEZESCU, A.M., CRISTESCU, R., CHIFIRIUC, M.C., DORCIOMAN, G., SOCOL, G., MIHAILESCU, I.N., MIHAIESCU, D.E., FICAI, A., VASILE, O.R., ENCULESCU, M., CHRISEY, D.B., Biofabrication, **7**, 2015, art. no. 015014.
10.CHEN, Z., XU, W., JIN, L., ZHA, J., TAO, T., LIN, Y., WANG, Z., J. Mater. Chem. A., **2**, 2014, p. 18339.
11.ANBARASU, M., ANANDAN, M., CHINNASAMY, E., GOPINATH, V., BALAMURUGAN, K., Spectrochim. Acta. Part. A. Mol. Biomol. Spectrosc., **135**, 2015, p. 536.
12. TAI, M.F., LAI, C.W., ABDUL HAMID, S.B., J. Nanomater., **2016,** 2016, p. 1.
13. SCHWAMINGER, S.P., GARCÍA, P.F., MERCK, G.K., BODENSTEINER, F.A., HEISSLER, S., GUNTHER, S., BERENSMEIER, S., J. Phys. Chem C., **119**, 2015, p. 23032.
14. TIE, S.L., LIN, Y.Q., LEE, H.C., BAE, Y.S., LEE, C.H., Colloids Surf. A. Physicochem. Eng. Asp. **273**, 2006, p. 75.
15. REHANA, D., HALEEL, A.K., RAHIMAN, A.K., J. Chem. Sci., **127**, 2015, p. 1155.
16. CIRCU, M., NAN, A., BORODI, G., LIEBSCHER, J., TURCU, R., Nanomater., **6**, 2016, p. 228.

Manuscript received: 4.04.2019